Article

Solar Still Efficiency Enhancement by Using Graphene Oxide/Paraffin Nano-PCM

Mohammad Reza Safaei [1,2] , **Hamid Reza Goshayeshi [3,*]** and **Issa Chaer [4]**

[1] Division of Computational Physics, Institute for Computational Science, Ton Duc Thang University, Ho Chi Minh City 758307, Vietnam; cfd_safaei@tdtu.edu.vn

[2] Faculty of Electrical and Electronics Engineering, Ton Duc Thang University, Ho Chi Minh City 758307, Vietnam

[3] Department of Mechanical Engineering, Mashhad Branch, Islamic Azad University, Mashhad 918714757, Iran

[4] Centre for Civil and Building Service Engineering, School of the Built Environment and Architecture, London South Bank University, London SE1 0AA, UK; chaeri@lsbu.ac.uk

* Correspondence: goshayshi@yahoo.com

Abstract: Solar-driven water desalination technologies are rapidly developing with various links to other renewable sources. However, the efficiency of such systems severely depends on the design parameters. The present study focused on using graphene oxide (GO) with the Φ = 0.2, 0.4 and 0.6 wt.% dispersed in paraffin, as phase-change materials (PCMs), to improve the productivity of a solar still for desalination applications. The outcomes showed that by adding more graphene oxide to paraffin, the melting temperature got reduced. Solar still with GO/paraffin showed 25% productivity improvement in comparison with the solar still with only PCM. The obtained Nusselt number during the melting time also represented that free convection heat transfer into the melted region of the solar still has been enhanced by adding dispersed GO to the PCM, compared to the base paraffin. Also, increasing the hot wall temperature augments the Nusselt number. Finally, an empirical equation was derived to correlate the average Nusselt number as a function of Rayleigh number (Ra), the Stefan number (Ste), the subcooling factor (Sb), and the Fourier number (Fo). The obtained correlation depicted that Nusselt number enhancement has a reverse relation with Fourier number.

**Keywords:** solar still; phase-change material; experimental study; graphene oxide

1. Introduction

Over the latest decades, phase-change materials (PCMs) have been employed in the heat transfer systems like solar stills [1–3]. As is clear from Figure 1, phase-change materials are categorized as Eutectic, inorganic, and organic [4].

Among the variety of proposed PCMs, paraffin, as an organic material, is evaluated as one of the most futuristic PCMs, due to its desired specifications, like remarkable latent heat [5–7]. As an example, Kumar et al. [8] enhanced the productivity of a traditional solar still by employing paraffin and attaching some fins. Their results revealed that the daily and night-time exergy efficiency of the modified solar still is augmented by 20% and 74%, respectively. In a similar work, Kabeel and Abdelgaied [9] utilized the paraffin in a solar still in Egypt. Their outcomes demonstrated that paraffin is a decisive factor in water productivity of the solar still, as it can increase it up to 67.18%. However, low thermal conductivity of paraffin causes lower heat transfer rates within melting process [10]. For improving the heat transfer rate of PCMs, different solutions have been proposed in the literature. In recent years, the concept of nanofluids was considered among researchers to improve the thermal conductivity of

the phase-change materials, by dispersing the nanomaterials into the base PCMs [11,12]. Considering these facts, paraffin is a good candidate for using in solar stills. However, its low conductivity problem can be reduced by adding nanoparticles [13,14].

Table 1 shows the synopsis of the investigations about different nano-paraffin composites. As can be seen from the table, graphene-based nanomaterials have a promising potential to enhance the thermal conductivity of paraffin.
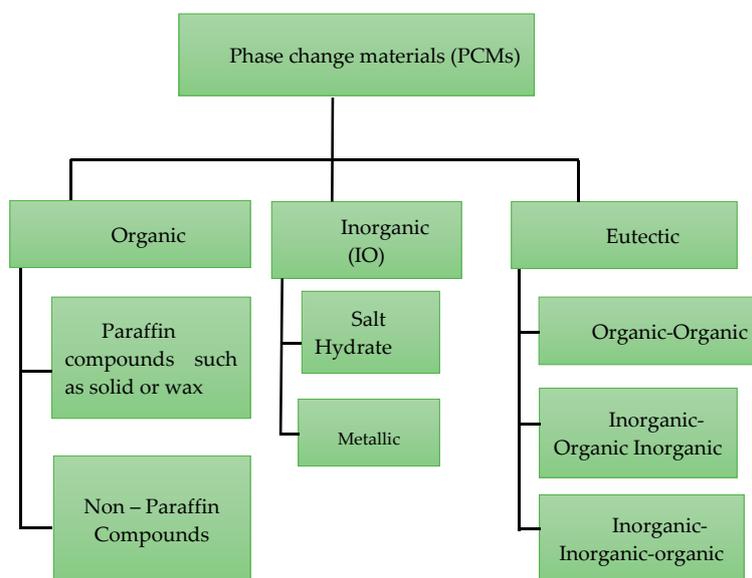
Figure 1. Classification of phase-change materials (PCMs) [4]. Figure is reprinted with permission from publisher.

Table 1. Synopsis of the investigations about different nano-paraffin composites.

Author	Used Nanomaterials	Results
Rufuss et al. [15]	Copper (II) oxide	35% improvement in the productivity.
Sahan et al. [16]	Iron (II,III) oxide	Thermal conductivity of paraffin raised by 48% and 60%, by employing 10% and 20% wt.% of Fe_3O_4 nanoparticles.
Jiang et al. [17]	Aluminum oxide	15% latent heat decrement and 27% thermal conductivity increment.
Yang et al. [18]	Silicon Nitride	Thermal conductivity rising by 35%, utilizing 10% nanoparticles.
Park et al. [19]	Iron (II,III) oxide	45% latent heat decrement and 45% thermal conductivity enhancement by dispersing 6.6% nanoparticles in the base PCM.
Fan et al. [20]	Graphene	164% thermal conductivity increment, by dispersing 5% nanomaterials in the paraffin.
Jesumatty et al. [21]	Copper (II) oxide	6%, 6.7%, and 7.8% thermal conductivity augmentation, by dispersing 2%, 5%, and 10% nanoparticles in the base PCM.
Shi et al. [22]	Graphite nanoplatelets	Augmenting the thermal conductivity of PCM from 0.25 to 2.7, by dispersing 10% of nanomaterial in the base PCM.
Nourani et al. [23]	Aluminum oxide	Adding 10% nanoparticles to the base paraffin afford a 0.09 W/m °C thermal conductivity improvement.
Li [24]	Graphite	Adding 10% graphite nanomaterial to the base PCM, cause a 640.43% thermal conductivity enhancement.
Warzoha et al. [25]	Graphite nanofibers	180% thermal conductivity increase and 10% latent heat decrease by adding 11.4% graphite nanofibers to the base paraffin.

Although many researches have focused on thermal enhancement of nanofluids by adding more nanomaterials to the base fluid [26,27], present study has concentrated on using paraffin with dispersed graphene oxide with the Φ =0.2, 0.4, and 0.6% to improve the productivity of a solar still. The outcome of this investigation may find applications to develop highly efficient solar stills to secure more drinkable water in warm, dry lands [28–32].

2. Experimental

2.1. Thermophysical Properties

Paraffin wax (industrial grade) purchased from Merck company (Gernsheim, Germany), with melting temperature of 44 °C was employed as the PCM. Also, graphene oxide nanomaterial was purchased from US Research Nanomaterials, Inc. to be used as an additive to PCM to improve its thermal performance. Thermal properties of PCM and graphene oxide have been shown in Table 2.

Table 2. Thermal properties of PCM and graphene oxide.

Thermophysical Property	Paraffin	Graphene Oxide
Density (kg/m^3)	802	3600
Specific heat (J/kg K)	2320 (liquid)	765
Thermal conductivity (W/m K)	0.23 (liquid)	3000
Dynamic viscosity (kg/m s)	1.3×10^{-3}	-
Thermal expansion coefficient (1/K)	9.1×10^{-4}	1.25×10^{-5}
Latent heat (kJ/kg)	226	-
Melting temperature (°C)	44	-

The thermophysical properties of the nano-PCM can be calculated using below equations [33,34]:

$$\rho_{npcm} = \varnothing \rho_{np} + (1 - \varnothing)_{\rho cm} \tag{1}$$

$$c_{p,npcm} = \frac{\varnothing \left(\rho c_p\right)_{np} + (1 - \varnothing)\left(\rho c_p\right)_{pcm}}{\rho_{npcm}} \tag{2}$$

$$h_{fg\ npcm} = \frac{(1 - \varnothing)\left(\rho h_{fg}\right)_{pcm}}{\rho_{npcm}} \tag{3}$$

The dynamic viscosity of the nano-PCM can be obtained by [35,36]:

$$\mu_{npcm} = 0.983 e^{12.959 \varnothing} \mu_{pcm} \tag{4}$$

The thermal conductivity of the nano-PCM, subject to Brownian motion, is defined as [35]:

$$k_{npcm} = \frac{k_{np} + 2k_{pcm} - 2\left(k_{pcm} - k_{np}\right)\varnothing}{k_{np} + 2k_{pcm} + 2\left(k_{pcm} - k_{np}\right)\varnothing} k_{pcm} + 5 \times 10^4 \beta_k \zeta \phi \rho_{pcm} c_{p,pcm} \sqrt{\frac{BT}{\rho_{np} d_{np}}} f(T, \phi) \tag{5}$$

where β is the Boltzmann constant, 1.381×10^{-23} J/K and

$$\begin{aligned}
\beta_k &= 8.4407(100\phi)^{-1.07304} \\
\beta &= 0 \qquad if\ T < T_{solidus} \\
\beta &= 1 \qquad if\ T < T_{liquidus}
\end{aligned} \tag{6}$$

ζ is the correction factor and is defined as [37]:

$$\zeta = \frac{T - T_{solid}}{T_{liquid} - T_{solid}} \qquad if\ T_{solidus} < T_{liquidus} \tag{7}$$

f is a function, which can be defined as [36]:

$$f(T, \varnothing) = \left(2.8217 \times 10^{-2}\varnothing + 3.917 \times 10^{-3}\right)\frac{T}{T_{ref}} + \left(-3.0669 \times 10^{-2}\varnothing - 3.91123 \times 10^{-3}\right) \tag{8}$$

Paraffin and graphene oxide used in the present study can be seen in Figure 2.

(a)   (b)

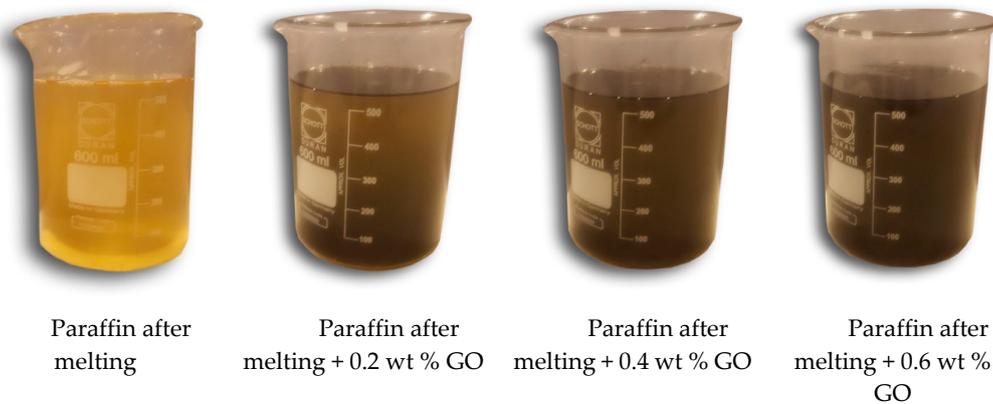**Figure 2.** Materials used in the present study—(**a**) paraffin and (**b**) graphene oxide.

2.2. Preparation of the Nanocomposite

Figure 3 demonstrates the nanocomposite preparation. The black plate receives heat by radiation during the day time. As a result, this heat will be transferred to the paraffin/graphene oxide. The present study focused on using graphene oxide (GO) with the $\Phi = 0.2, 0.4,$ and 0.6 wt.% dispersed into melted paraffin at the temperature of 45 °C, as phase-change materials (PCMs), to improve the productivity of a solar still. Mixing was applied for 2 h with 95% power intermittently to prevent overheating of the nanofluid. During the day time, especially after 2 p.m., paraffin starts to melt, and its temperature remains constant until the melting is complete. After 7 p.m., paraffin starts to cool, but the temperature remains constant until all the paraffin becomes solid; then cools back to the surrounding temperature. During the day time, when no paraffin exists, the water temperature is high, but after 7 p.m., T_w with PCM is higher. A thin layer of paraffin/graphene oxide has been integrated beneath the basin (as shown in Figure 3) to increase the efficiency of solar still during the night time.
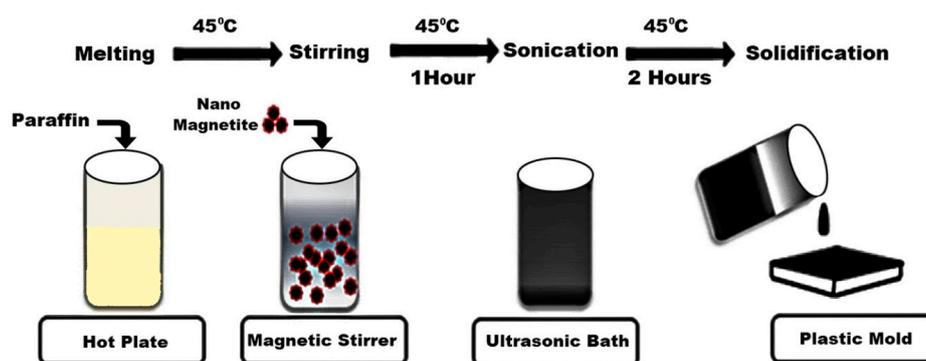
Figure 3. Steps of preparation of paraffin/graphene oxide.

Figure 4 also provides sedimentation level pictures of the prepared suspension. As is clear from the figure, the graphene oxide can disperse in the organic solvents easily, without any noticeable sedimentation.

| Paraffin after melting | Paraffin after melting + 0.2 wt % GO | Paraffin after melting + 0.4 wt % GO | Paraffin after melting + 0.6 wt % GO |

Figure 4. Visualization of prepared paraffin/graphene oxide.

2.3. Experimental Apparatus

Figure 5 demonstrates the picture as well as schematic of the studied solar still. The experimental setup includes two parts, a solar still and an effluent settling tank. The solar still is the main part of the experiments and the effluent settling tank is used to eliminate any possible bacteria.

This settling tank is made from galvanized iron sheets with a diameter of 50 cm and a height of 60 cm. For enhancing the surface contact area, three rectangular fins ($40 \times 80 \times 1$ mm) are welded at the bottom of the tank basin. The settled effluent from the storage tank is traversed to the solar still.

The test unit comprised of a stepped-type solar absorber plate was installed on a metal base. The absorber plate was manufactured from galvanized iron sheet of 1 mm thick and 1300 mm length and 1000 mm width, which was coated with black color paint. The gap between the stepped absorber plate and the box was covered with polyurethane foam (PUF) to prevent heat loss from the sides and bottom of the unit. The cover is made of 4 mm thick glass. Raw water was used for the tests, flowing from the tank, down the steps of an absorber. This water is warmed by solar radiation and therefore, it evaporated. The vapor was condensed at the inner glass surface and the droplets were slid along the glass. Gathered water dripped to the distilled water container at the bottom, and collected in a beaker. This was done by a pipe that was installed on the side of the unit. The makeup water was refilled every 30 min, by opening a valve to keep a constant concentration for the water. Excess saline water flowed through the absorber into the tank.

It is noteworthy that one of the factors influencing the production rate is the slope of the roof, which is a function of latitude, the angle of the solar radiation, and the seasons of the year [38]. As a rule of thumb, the angle is considered equal to the latitude [39]. For the studied city, the latitude is 36.31° [40]. The most proper direction for the installation of solar panels that are deployed on a fixed basis is geographic east–west direction [41]. In the northern hemisphere, the unit must be headed toward the south; so that solar energy could be best exploited. Experiments are performed from 8 a.m. to 6 p.m., during July 2018–August 2018.

Three different thermocouples were installed to measure the temperature of the absorbent plate (T_b), the temperature of the inner surface of the glass (T_{gi}) and temperature of water desalination unit (T_w). For monitoring evaporator and condenser surface temperature, a set of K-type thermocouples were used, which were connected to a portable data logger. The uncertainty in the measurement of temperature was equal to ±1 K, according to the temperature monitoring system. The environment, basin plate, solution and glass temperatures as well as solar radiation and distilled water productivity were measured every 1 h.
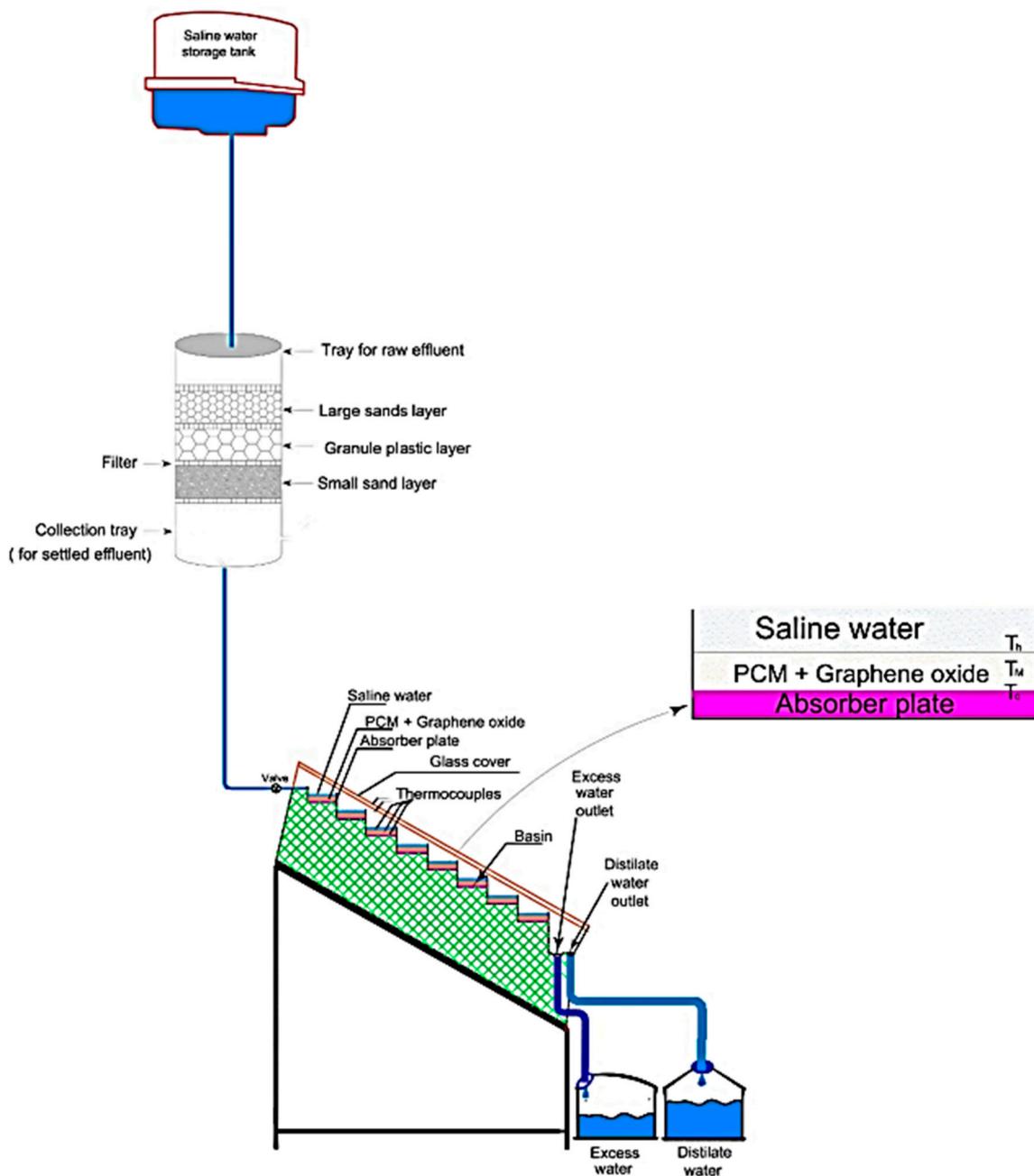
Figure 5. Schematics of utilized solar still.

Table 3 presents a summary of design specifications of the solar stills.

Table 3. Design parameters for the studied solar still.

| Parameters	Dimensions
Length of tank	600 mm
Width of tank	400 mm
Height of tank	2800 mm
Inclination angles	32.5°
Length of the glass covers	1300 mm
Width of the glass covers	1000 mm
Thickness of the glass covers	4 mm

Uncertainties

Errors of the measuring instruments are displayed in Table 4. These errors have been indicated, based on the manufacturer's instructions.

Table 4. The accuracies of various measurement instruments [42]. Table is reprinted with permission from publisher.

No.	Instrument	Range	Accuracy	% Error
1	Solarimeter	0–900 W/m^2	±4 W/m^2	5
2	Thermocouple	0–300 °C	±1 °C	4
3	Thermometer	0–95 °C	±0.1 °C	0.4
4	Anemometer	0–12 m/s	±0.1 m/s	10
5	Measuring jar	0–1000 mL	±9 mL	9

3. Results and Discussion

Experimental investigation was performed to study the thermal performance of GO/PCM in solar still. During the day time, solar energy can be divided between the water, which we wanted to distill, and the PCM/ graphene oxide. As is clear from Figure 6, water temperature without PCM is the highest between 9 a.m. and 12 p.m., as during this time, a part of solar energy is stored in PCM. After that and for no-PCM case, the temperature got reduced sharply but temperature for solar still with paraffin diminished gradually. This is because the stored energy in PCM is released, when the sun sets. Adding more nanomaterials to the base PCM caused higher temperature for the time duration from 2 p.m. to 7 p.m.
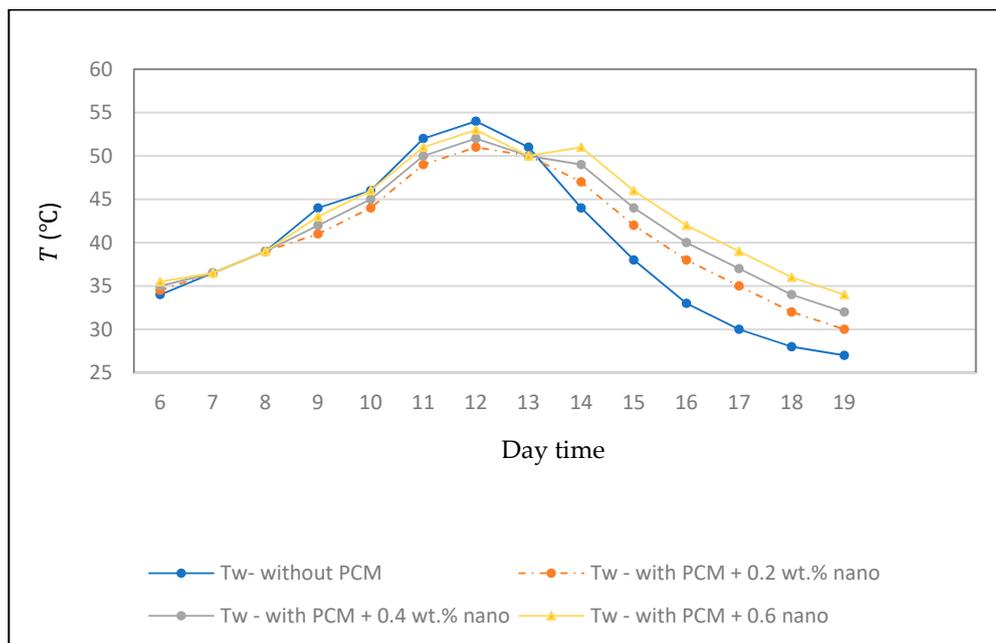
Figure 6. Comparison between temperatures in the presence and absence of PCM and nano-PCMs.

The distillation amount is the primary factor in determining the performance of a solar desalination system. The volume of the existing water varies due to different utilized nanocomposites in solar still system. Figure 7 illustrated the produced fresh water per day time. The figure shows that adding more GO to paraffin causes more fresh water production which indicates solar still efficiency enhancement. The reason of this phenomenon is related to the ability of nano-PCM to make the basin water warmer, which means more water can be distilled. Also, with nano-PCM energy released during the sunset, the distilled water production still continued. All of these reasons caused the maximum production at the end of the day to have about 100% enhancement.
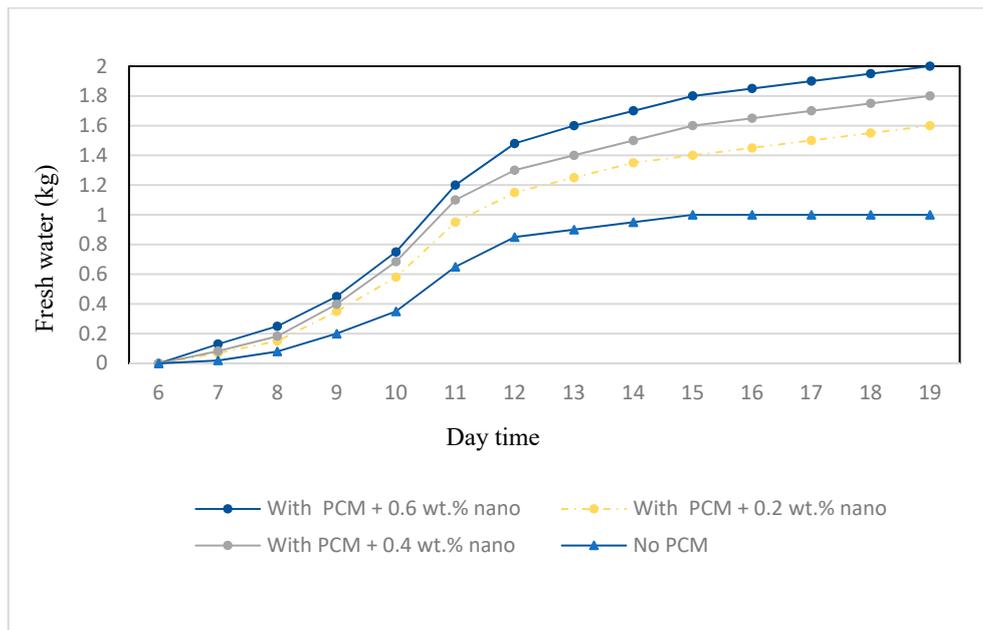
Figure 7. Produced fresh water in the presence and absence of PCM and nano-PCMs.

Figure 8 shows the alteration of the average Nusselt number at the hot wall, while the cold bottom surface is at 23 °C. As is evident, the Nusselt number follows the same trend of previous investigations like [43]. Adding more GO to the base paraffin enhances the average Nusselt number. This is owing to the thermal conductivity increment of PCMs, by dispersing nanomaterials in them. Also, increasing the Fourier number reduces the average Nusselt number.

The mean Nusselt number based on a recent obtained correlation [43,44] can be written as below:

$$\overline{Nu} = 0.18\left(\frac{Pr}{0.2 + Pr}Ra\right)^{0.29} \tag{9}$$

Also, the mean heat transfer coefficient can be given as:

$$\overline{h} = \frac{\overline{Nu}k_m}{H} \tag{10}$$

The Rayleigh and the Stefan numbers can be defined based on the temperature difference in the melted zone and the characteristic length of the solar still [45]:

$$Ra_f = \frac{g\rho_f^2 c_{\rho.f}\beta_f(T_h - T_c)H^3}{k_f\mu_f} \tag{11}$$

$$Ra_m = \frac{g\rho_f^2 c_{\rho.f}\beta_f(T_h - T_c)H^3}{k_m\mu_m} \tag{12}$$

and

$$Ste_f = \frac{c_{\rho.f}(T_h - T_c)}{h_{ls.f}} \tag{13}$$

$$Ste_m = \frac{c_{\rho.m}(T_h - T_c)}{h_{ls.m}} \tag{14}$$
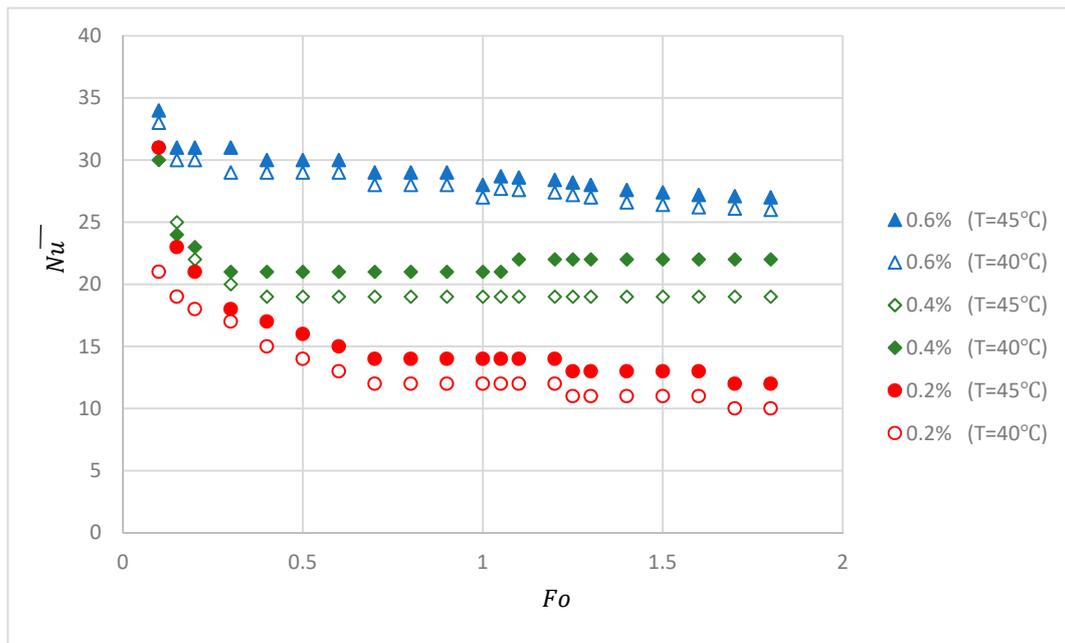
Figure 8. Efficacy of hot wall temperature on the average Nusselt number.

In the final step, an empirical correlation according to the experimental outcomes has been developed to correlate the average Nusselt number in relation to the Rayleigh number (Ra), the Stefan number (Ste), the subcooling factor (Sb) and the Fourier number (Fo) by using the below formula:

$$\overline{Nu} = aRa_m^b \left[\frac{Ste_m Fo_m}{(1 + Sb)} \right]^c \tag{15}$$

This formula is similar to that reported by Ho and Gao [43] for Al_2O_3/paraffin nano-PCM. To obtain the constant variables of the equation, a dataset was used to compute the variables by using Microsoft Excel. Least square regression method was employed to acquire the correlation values based on the dataset points. The values of variables in Equation (15) for studied dispersed amounts of nanoparticle into the PCM are shown in Table 5.

Table 5. Coefficient, exponents and ranges of parameters for Equation (15).

Φ	a	b	c	Average Deviation (%)	Parameter Ranges
0%	0.6	0.3	−0.2	4.23	$Fo_m = 0.25\text{–}2.5;$ $Ra_m = 1.32 \times 10^6\text{–}2.38 \times 10^6$ $Sb = 0.075\text{–}0.85;$ $Ste_m = 0.05\text{–}0.2;$
0.2%	0.65	0.35	−0.23	7	$Fo_m = 0.25\text{–}2.5;$ $Ra_m = 2.59 \times 10^6\text{–}4.85 \times 10^6$ $Sb = 0.075\text{–}0.85;$ $Ste_m = 0.05\text{–}0.2;$
0.4%	0.7	0.4	−0.3	9	$Fo_m = 0.25\text{–}2.5;$ $Ra_m = 5.13 \times 10^6\text{–}5.49 \times 10^6$ $Sb = 0.075\text{–}0.85;$ $Ste_m = 0.05\text{–}0.2;$
0.6%	0.8	0.5	−0.4	10.5	$Fo_m = 0.25\text{–}2.5;$ $Ra_m = 3.76 \times 10^6\text{–}7.21 \times 10^6$ $Sb = 0.075\text{–}0.85;$ $Ste_m = 0.05\text{–}0.2.$

4. Conclusions

In this research, graphene oxide nanomaterials with Φ = 0.2, 0.4, and 0.6 wt.% are dispersed in paraffin (GO/PCM) and utilized in a solar still for desalination applications. Based on the outcomes, following points were summarized:

1. Solar still efficiency with GO/paraffin showed an average of 25% improvement compared to the solar still with only PCM.

2. The daily productivity of solar still with PCM was 2 kg/0.4 m^2 whilst the solar still with Φ = 0.6 wt.% GO/ PCM yielded 2.5 kg/0.4 m^2.

3. Adding more GO to PCM caused higher Nusselt number and consequently higher heat transfer coefficient, which means high potential to obtain remarkable reduction in heating times. However, the samples containing 0.2 wt.% nanomaterial showed least performance levels in feasible energy storage during phase change.

4. Dispersed graphene-based nanomaterials in paraffin exhibits better potential, compared to the use of raw PCMs in solar applications.

5. An empirical equation has been derived to correlate the average Nusselt number as a function of Rayleigh number, the Stefan number, the Fourier number, and the subcooling factor.

Nomenclature

A	heat transfer area, m^2
B	Boltzmann constant, $(1.3807 \times 10^{-23}$ J/K)
C_p	specific heat, J/(kg K)
Fo_f	Fourier number, $\alpha_f t / H^2$
g	gravitational acceleration, m/s^2
h_{ls}	latent heat of fusion, kJ/kg
h	heat transfer coefficient in paraffin + nanomaterial (W/m^2.K)
H	height, m
k	thermal conductivity, W/m k
L	depth, m
Nu	Nusselt number
q_h	heat transfer rate at the hot wall, W
Ra_f	Rayleigh Number, $g\beta_f (T_h - T_c)H^3/(\alpha_f v_f)$
Sb	subcooling parameter, $(T_h - T_c)/(T_M - T_c)$
Ste_f	Stefan number, $c_{\rho,f}(T_h - T_c)/h_{ls,f}$
T	temperature, °C
W	width, m
GO	graphene oxide
PCM	phase-change material
Greek symbols	
α	thermal diffusivity, m^2/s
β	thermal expansion coefficient, 1/K
μ	dynamic viscosity Ns/m^2
ρ	density, kg/m^3
Φ	Percent of nanomaterial
ζ	correction factor (-)

Subscripts

air	air
C	cold wall
f	base fluid
h	hot surface
m	quantities for dispersed nanomaterial in the paraffin emulsion
M	average temperature of PCM

References

1. Asbik, M.; Ansari, O.; Bah, A.; Zari, N.; Mimet, A.; El-Ghetany, H. Exergy analysis of solar desalination still combined with heat storage system using phase change material (PCM). *Desalination* **2016**, *381*, 26–37. [CrossRef]

2. Faegh, M.; Shafii, M.B. Experimental investigation of a solar still equipped with an external heat storage system using phase change materials and heat pipes. *Desalination* **2017**, *409*, 128–135. [CrossRef]

3. Pandey, A.; Hossain, M.; Tyagi, V.; Rahim, N.A.; Jeyraj, A.; Selvaraj, L.; Sari, A. Novel approaches and recent developments on potential applications of phase change materials in solar energy. *Renew. Sustain. Energy Rev.* **2018**, *82*, 281–323.

4. Sharma, A.; Tyagi, V.V.; Chen, C.R.; Buddhi, D. Review on thermal energy storage with phase change materials and applications. *Renew. Sustain. Energy Rev.* **2009**, *13*, 318–345. [CrossRef]

5. Safari, A.; Saidur, R.; Sulaiman, F.; Xu, Y.; Dong, J. A review on supercooling of Phase Change Materials in thermal energy storage systems. *Renew. Sustain. Energy Rev.* **2017**, *70*, 905–919. [CrossRef]

6. Zhou, Q.; Liu, P.-F.; Tzeng, C.-T.; Lai, C.-M. Thermal Performance of Microencapsulated Phase Change Material (mPCM) in Roof Modules during Daily Operation. *Energies* **2018**, *11*, 679. [CrossRef]

7. Li, S.; Chen, Y.; Sun, Z. Numerical simulation and optimization of the melting process of phase change material inside horizontal annulus. *Energies* **2017**, *10*, 1249.

8. Kumar, T.S.; Jegadheeswaran, S.; Chandramohan, P. Performance investigation on fin type solar still with paraffin wax as energy storage media. *J. Therm. Anal. Calorim.* **2019**, *136*, 101–112. [CrossRef]

9. Kabeel, A.E.; Abdelgaied, M. Improving the performance of solar still by using PCM as a thermal storage medium under Egyptian conditions. *Desalination* **2016**, *383*, 22–28. [CrossRef]

10. Mohamed, S.A.; Al-Sulaiman, F.A.; Ibrahim, N.I.; Zahir, M.H.; Al-Ahmed, A.; Saidur, R.; Yılbaş, B.; Sahin, A. A review on current status and challenges of inorganic phase change materials for thermal energy storage systems. *Renew. Sustain. Energy Rev.* **2017**, *70*, 1072–1089. [CrossRef]

11. Chieruzzi, M.; Cerritelli, G.F.; Miliozzi, A.; Kenny, J.M. Effect of nanoparticles on heat capacity of nanofluids based on molten salts as PCM for thermal energy storage. *Nanoscale Res. Lett.* **2013**, *8*, 448. [CrossRef]

12. Olia, H.; Torabi, M.; Bahiraei, M.; Ahmadi, M.H.; Goodarzi, M.; Safaei, M.R. Application of nanofluids in thermal performance enhancement of parabolic trough solar collector: state-of-the-art. *Appl. Sci.* **2019**, *9*, 463. [CrossRef]

13. Sheikholeslami, M. Numerical simulation for solidification in a LHTESS by means of nano-enhanced PCM. *J. Taiwan Inst. Chem. Eng.* **2018**, *86*, 25–41. [CrossRef]

14. Shahsavar, A.; Khanmohammadi, S.; Karimipour, A.; Goodarzi, M. A novel comprehensive experimental study concerned synthesizes and prepare liquid paraffin-Fe_3O_4 mixture to develop models for both thermal conductivity & viscosity: A new approach of GMDH type of neural network. *Int. J. Heat Mass Transf.* **2019**, *131*, 432–441.

15. Rufuss, D.D.W.; Iniyan, S.; Suganthi, L.; Davies, P. Nanoparticles enhanced phase change material (NPCM) as heat storage in solar still application for productivity enhancement. *Energy Procedia* **2017**, *141*, 45–49. [CrossRef]

16. Şahan, N.; Fois, M.; Paksoy, H. Improving thermal conductivity phase change materials—A study of paraffin nanomagnetite composites. *Sol. Energy Mater. Sol. Cells* **2015**, *137*, 61–67. [CrossRef]

17. Jiang, X.; Luo, R.; Peng, F.; Fang, Y.; Akiyama, T.; Wang, S. Synthesis, characterization and thermal properties of paraffin microcapsules modified with nano-Al_2O_3. *Appl. Energy* **2015**, *137*, 731–737. [CrossRef]

18. Yang, Y.; Luo, J.; Song, G.; Liu, Y.; Tang, G. The experimental exploration of nano-Si_3N_4/paraffin on thermal behavior of phase change materials. *Thermochim. Acta* **2014**, *597*, 101–106. [CrossRef]

19. Park, S.; Lee, Y.; Kim, Y.S.; Lee, H.M.; Kim, J.H.; Cheong, I.W.; Koh, W.-G. Magnetic nanoparticle-embedded PCM nanocapsules based on paraffin core and polyurea shell. *Colloids Surf. A Physicochem. Eng. Asp.* **2014**, *450*, 46–51. [CrossRef]

20. Fan, L.-W.; Fang, X.; Wang, X.; Zeng, Y.; Xiao, Y.-Q.; Yu, Z.-T.; Xu, X.; Hu, Y.-C.; Cen, K.-F. Effects of various carbon nanofillers on the thermal conductivity and energy storage properties of paraffin-based nanocomposite phase change materials. *Appl. Energy* **2013**, *110*, 163–172. [CrossRef]

21. Jesumathy, S.; Udayakumar, M.; Suresh, S. Experimental study of enhanced heat transfer by addition of CuO nanoparticle. *Heat Mass Transf.* **2012**, *48*, 965–978. [CrossRef]

22. Shi, J.-N.; Ger, M.-D.; Liu, Y.-M.; Fan, Y.-C.; Wen, N.-T.; Lin, C.-K.; Pu, N.-W. Improving the thermal conductivity and shape-stabilization of phase change materials using nanographite additives. *Carbon* **2013**, *51*, 365–372. [CrossRef]

23. Nourani, M.; Hamdami, N.; Keramat, J.; Moheb, A.; Shahedi, M. Thermal behavior of paraffin-nano-Al$_2$O$_3$ stabilized by sodium stearoyl lactylate as a stable phase change material with high thermal conductivity. *Renew. Energy* **2016**, *88*, 474–482. [CrossRef]

24. Li, M. A nano-graphite/paraffin phase change material with high thermal conductivity. *Appl. Energy* **2013**, *106*, 25–30. [CrossRef]

25. Warzoha, R.J.; Weigand, R.M.; Fleischer, A.S. Temperature-dependent thermal properties of a paraffin phase change material embedded with herringbone style graphite nanofibers. *Appl. Energy* **2015**, *137*, 716–725. [CrossRef]

26. Sarafraz, M.M.; Safaei, M.R. Diurnal thermal evaluation of an evacuated tube solar collector (ETSC) charged with graphene nanoplatelets-methanol nano-suspension. *Renew. Energy* **2019**, *142*, 364–372. [CrossRef]

27. Sarafraz, M.; Tlili, I.; Abdul Baseer, M.; Safaei, M.R. Potential of Solar Collectors for Clean Thermal Energy Production in Smart Cities using Nanofluids: Experimental Assessment and Efficiency Improvement. *Appl. Sci.* **2019**, *9*, 1877. [CrossRef]

28. Wang, R.; Jiang, L.; Ma, Z.; Gonzalez-Diaz, A.; Wang, Y.; Roskilly, A.P. Comparative Analysis of Small-Scale Organic Rankine Cycle Systems for Solar Energy Utilisation. *Energies* **2019**, *12*, 829. [CrossRef]

29. Rashidi, S.; Akar, S.; Bovand, M.; Ellahi, R. Volume of fluid model to simulate the nanofluid flow and entropy generation in a single slope solar still. *Renew. Energy* **2018**, *115*, 400–410. [CrossRef]

30. Bareschino, P.; Pepe, F.; Roselli, C.; Sasso, M.; Tariello, F. Desiccant-Based Air Handling Unit Alternatively Equipped with Three Hygroscopic Materials and Driven by Solar Energy. *Energies* **2019**, *12*, 1543. [CrossRef]

31. Akbarzadeh, M.; Rashidi, S.; Karimi, N.; Ellahi, R. Convection of heat and thermodynamic irreversibilities in two-phase, turbulent nanofluid flows in solar heaters by corrugated absorber plates. *Adv. Powder Technol.* **2018**, *29*, 2243–2254. [CrossRef]

32. Kim, S.; Lee, S.; Park, J.Y. Thermo-Fluid Dynamic Effects of the Radial Location of the Baffle Installed in a Solar Updraft Tower. *Energies* **2019**, *12*, 1340. [CrossRef]

33. Abdollahzadeh, M.; Esmaeilpour, M. Enhancement of phase change material (PCM) based latent heat storage system with nano fluid and wavy surface. *Int. J. Heat Mass Transf.* **2015**, *80*, 376–385. [CrossRef]

34. Sheikholeslami, M. Numerical modeling of nano enhanced PCM solidification in an enclosure with metallic fin. *J. Mol. Liq.* **2018**, *259*, 424–438. [CrossRef]

35. Vajjha, R.S.; Das, D.K.; Namburu, P.K. Numerical study of fluid dynamic and heat transfer performance of Al$_2$O$_3$ and CuO nanofluids in the flat tubes of a radiator. *Int. J. Heat Fluid Flow* **2010**, *31*, 613–621. [CrossRef]

36. Mahdi, J.M.; Nsofor, E.C. Solidification of a PCM with nanoparticles in triplex-tube thermal energy storage system. *Appl. Therm. Eng.* **2016**, *108*, 596–604. [CrossRef]

37. Arasu, A.V.; Mujumdar, A.S. Numerical study on melting of paraffin wax with Al$_2$O$_3$ in a square enclosure. *Int. Commun. Heat Mass Transf.* **2012**, *39*, 8–16. [CrossRef]

38. Shukla, A.K.; Sudhakar, K.; Baredar, P. Design, simulation and economic analysis of standalone roof top solar PV system in India. *Sol. Energy* **2016**, *136*, 437–449. [CrossRef]

39. Sint, N.K.C.; Choudhury, I.; Masjuki, H.H.; Aoyama, H. Theoretical analysis to determine the efficiency of a CuO-water nanofluid based-flat plate solar collector for domestic solar water heating system in Myanmar. *Sol. Energy* **2017**, *155*, 608–619. [CrossRef]

40. Kermani, M.; Goudarzi, G.; Shahsavani, A.; Dowlati, M.; Asl, F.B.; Karimzadeh, S.; Jokandan, S.F.; Aghaei, M.; Kakavandi, B.; Rastegarimehr, B. Estimation of short-term mortality and morbidity attributed to fine particulate matter in the ambient air of eight Iranian cities. *Ann. Glob. Health* **2018**, 84. [CrossRef]

41. Llorens, D. Which Direction Should Solar Panels Face? Available online: https://solarpowerrocks.com/solar-basics/which-direction-should-solar-panels-face/ (accessed on 31 March 2019).

42. Sampathkumar, K.; Senthilkumar, P. Utilization of solar water heater in a single basin solar still—An experimental study. *Desalination* **2012**, *297*, 8–19. [CrossRef]

43. Ho, C.J.; Gao, J.Y. An experimental study on melting heat transfer of paraffin dispersed with Al$_2$O$_3$ nanoparticles in a vertical enclosure. *Int. J. Heat Mass Transf.* **2013**, *62*, 2–8. [CrossRef]

44. Bergman, T.L.; Incropera, F.P.; DeWitt, D.P.; Lavine, A.S. *Fundamentals of Heat and Mass Transfer*; John Wiley & Sons: Hoboken, NJ, USA, 2011.

45. Ebadi, S.; Tasnim, S.H.; Aliabadi, A.A.; Mahmud, S. Melting of nano-PCM inside a cylindrical thermal energy storage system: Numerical study with experimental verification. *Energy Convers. Manag.* **2018**, *166*, 241–259. [CrossRef]